J Bionic Eng 17 (2020) 270–280
DOI: https://doi.org/10.1007/s42235-020-0021-8

Journal of Bionic Engineering
https://www.springer.com/journal/42235

Experimental Study on Frog-inspired Swimming Robot Based on Articulated Pneumatic Soft Actuator

Jizhuang Fan, Shuqi Wang, Qingguo Yu, Yanhe Zhu*

State Key Laboratory of Robotics and System, *Harbin Institute of Technology*, *Harbin* 150001, *China*

Abstract

This paper presents a frog-inspired swimming robot based on articulated pneumatic soft actuator. To realize the miniaturization of the robot and enhance its environmental adaptability, combined with the advantages and characteristics of soft materials, an articulated pneumatic soft actuator is designed based on analysis of a frog's propulsion characteristics. A structural model is established to analyse the mechanical properties of the soft actuator. With the goal of making full use of the driving torque of the actuator and enhancing the propulsion efficiency of the robot, the motion trajectories of each joint of the robot are planned. Based on the trajectory planning, the control strategy of the soft actuator is determined to realize the frog-like swimming of the robot. The torso size after assembly is 0.175 m × 0.100 m × 0.060 m, which realizes the miniaturization of the frog-inspired robot. During the movement of the robot, the torso moves stably and flexibly, and can realize continuous linear and turning movements. The rationality of the structure and trajectory planning are verified by prototype experiments.

Keywords: bionic robotic frog, articulated pneumatic soft actuator, trajectory planning, prototype experiment

1 Introduction

As representative amphibians, frogs have gradually attracted the attention of bionics because of their excellent athletic ability[1,2]. Frog-inspired robots have great research value. At present, many scholars have focused on frog-inspired jumping robots[3,4]. There are relatively few studies on frog-inspired swimming robots, mainly focusing on theoretical modeling analysis and swimming mechanisms[5–10]. The prototype structures of the frog-inspired robots that have been developed are relatively complicated, large in size and heavy in weight, and it is impossible to truly realize frog-like swimming for these robots[8,11]. In addition, the rigid part of a robot is easily damaged when it comes into contact with the external environment, and the adaptability to the environment is relatively weak[12].

In recent years, soft structures have attracted the attention of researchers because of their environmental adaptability and human-computer interaction security superior to that of traditional rigid robots[13,14]. Therefore, researchers have carried out gradual and in-depth research and have achieved remarkable results for soft robots and their structural design[15–17]. The application of lightweight soft materials with good adaptability can better solve the above problems and greatly improve the adaptability of a robot to the environment while simplifying the body mechanism[18,19]. Additionally, the use of a soft actuator as a driving unit contributes to miniaturization, which is of great significance for the development of frog-inspired robots.

In addition, trajectory planning will help greatly improve the motion performance of a robot[20–22]. Based on motion analysis of bionic prototypes, kinematics has been used by many scholars for trajectory planning[23,24]. However, a real frog's trajectory is the result of long-term adaptation of its musculoskeletal system, with natural optimal characteristics[25]. The joint movement of frogs has the characteristics of long explosive duration and large range of motion. To realize bionic swimming for a frog-inspired robot, an articulated pneumatic soft actuator is prepared in combination with a soft material and is used as the connector and the driving part of the robot's limbs. Different forms of motion can be realized by rationally designing the structure of the soft actuator[26,27]. Based on characteris-

***Corresponding author:** Yanhe Zhu
E-mail: yhzhu@hit.edu.cn

tic analysis of the articulated pneumatic soft actuator, the trajectory of the frog-inspired robot is planned. The control process is determined by trajectory planning, and a bionic swimming movement that can reflect the characteristics of a real breaststroke is realized. The performance of the robot is tested by prototype experiments, which lay the foundation for research and further development of the frog-inspired amphibian robot. Importantly, the fusion application of rigid and soft material properties will make the frog-inspired robot have broader application prospects.

The rest of this paper is organized as follows: A structural model of the articulated pneumatic soft actuator and its characteristics are analyzed in section **2**. The motion trajectory is planned in section **3**. In section **4**, prototype experiments are carried out to verify the rationality of the performance of the robot. Finally, the conclusion and future work are given in section **5**.

2 Materials and methods

2.1 Structural model

To realize the miniaturization of the robot and bionic swimming, a frog-inspired swimming robot based on an articulated pneumatic soft actuator is designed. The skeletal system of a frog is shown in Fig. 1a[25]. The basic dimensions of the limbs are as follows: big arm (12.5 mm), arm (12.5 mm), thigh (28 mm), calf (27.5 mm), tibia (15 mm), the length of the sole and flipper is approximately 47 mm. The joint angles of the hip joint adduction, abduction and rotational motion are −45° – 90°, 40° – 140° and −50° – 50°, respectively. The flexion and extension motion angles of the knee joint, ankle joint and tarsometatarsal joint are 0° – 155°, −150° – 0° and −10° – 140°, respectively. By analyzing the angle of each joint, the limit of motion between adjacent limbs should not be less than 155° to meet the motion requirements of the robot.

The swimming characteristics of a frog are analyzed by a swimming observation experiment[28]; combined with the skeletal structure of the frog, the overall structural design scheme of the frog-inspired swimming robot shown in Fig. 1b is initially determined. The robot's torso and limbs are three times longer than those of a leopard frog. The joints are all driven by articulated pneumatic soft actuators, and the propulsive force and restoring force are generated by the coordinated movement of the actuators, thereby realizing bionic swimming of the robot.

Since the joints of the robot are in a contracted state before swimming, the initial shape of the articulated pneumatic soft actuator is designed as a semi-annular shape, as shown in Fig. 2a, and is composed of an elastic matrix, a strain-limiting layer, a fibre line, a sealing obstructing head, and a gas guiding head. The cross-sectional shape of the inner cavity is designed to be rectangular. The strain difference between the strain-limiting layer and the elastic matrix is used to achieve a progressively decreasing centre angle motion. When filled with compressed gas, the torque generated by the articulated pneumatic soft actuator can drive a limb to realize a stroke action. When the pressure is released, the torque generated by the elastic matrix of the actuator can restore the limb to achieve a recovery action. This is just enough to meet the more vigorous stretching movement of the limbs during the propulsion phase, and a more gradual movement in the recovery phase. Therefore, the articulated pneumatic soft actuator not only serves as the connecting component but also serves as the driving unit of the frog-inspired swimming robot.

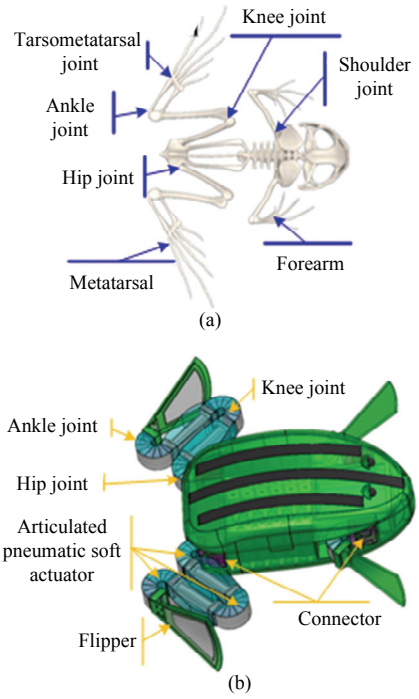

Fig. 1 The structures of the frog and the robot. (a) The skeletal structure of a real frog; (b) the overall structural design of the robot.

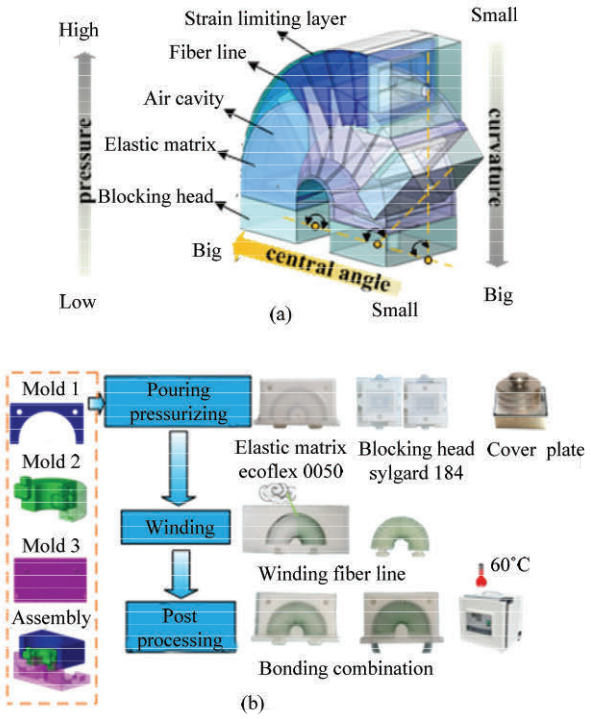

Fig. 2 The structural models of an articulated pneumatic soft actuator. (a) The center angle changes as the air pressure changes; (b) the entire process includes making molds, casting twice, winding fiber lines, and bonding.

This component is the key to meeting the movement demand and realizing a compact and lightweight structure.

The articulated pneumatic soft actuator consists of a number of different components that are selected according to their respective functional characteristics. Combining 3D printing, moulding and bonding techniques, the mould structure and fabrication process of the soft actuator are illustrated in Fig. 2b.

2.2 Characteristic analysis of the articulated pneumatic soft actuator

Due to the influence of the preparation process and the processed materials, there is a certain error between the theoretical analysis and the actual characteristics. The actual characteristics of the articulated pneumatic soft actuator are obtained by experimental tests and verify its feasibility, laying the foundation for its trajectory planning.

2.2.1 Motion characteristics

The test platform shown in Fig. 3 is designed to obtain the actual motion characteristics. The experimental operation of the soft actuator is pressurized and then gradually relieved. The host computer communicates with the MCU through the UART, and an electrical proportional valve is adjusted by the PWM to control the gas path. The internal pressure of the chamber is measured by an XGZP-type gas pressure sensor, and the bending angle of the actuator at the corresponding air pressure is measured by an RFP film-type bending sensor. The data collected by the sensor are sent to the MCU and transmitted to the host computer to obtain the current bending angle and air pressure.

2.2.2 Mechanical properties

The articulated pneumatic soft actuator is mainly used to generate the driving force and the restoring force. To better understand the mechanical properties of the actuator, the experimental platform and its experimental principles are shown in Fig. 4.

The two ends of the soft actuator are fixed by a digital display ruler, and the air pressure of the inner cavity is gradually increased, so that the characteristic relationship between the gas pressure P_{in} and the output driving torque M_D at different angles can be obtained. The bending angle is fixed from 40° to 70° in increments of 5°, and the P_{in}-M_D characteristic curve of the soft actuator is shown in Fig. 5. The characteristic curve changes approximately linearly within a certain load range.

3 Joint trajectory planning and actuator control strategy

A frog swims in the form of a swipe motion that is intermittent and highly explosive, so it is very important to plan the trajectory. The swimming process is simplified into three stages of advancement, sliding and recovery. The frog's joint angle is maintained during the sliding phase, and trajectory planning is not required[29,30]. Therefore, it is only necessary to perform trajectory planning for the propulsion and recovery stages based on the characteristic analysis of the soft actuator.

3.1 Joint trajectory planning during the propulsion stage

According to the structural characteristics of the frog-inspired swimming robot, the trajectory planning of

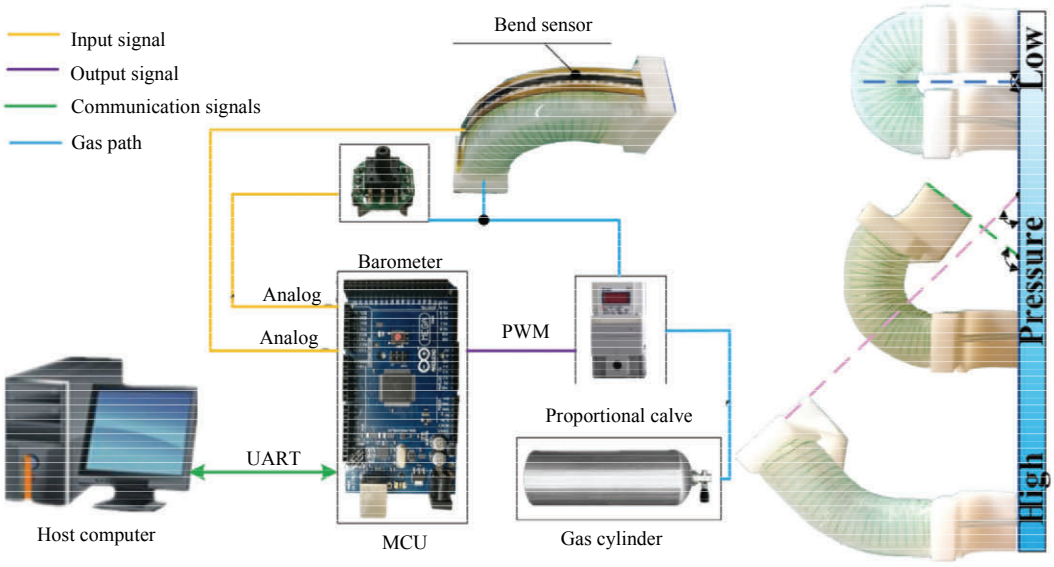

Fig. 3 The test platform for motion characteristics.

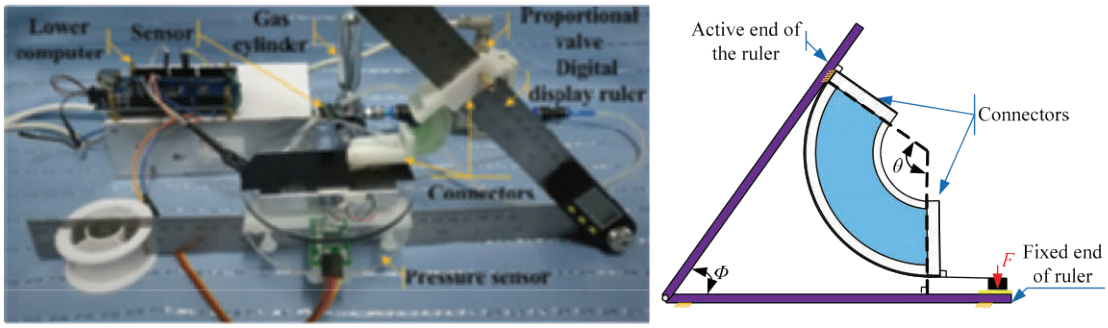

Fig. 4 The experimental device composition and its experimental principle.

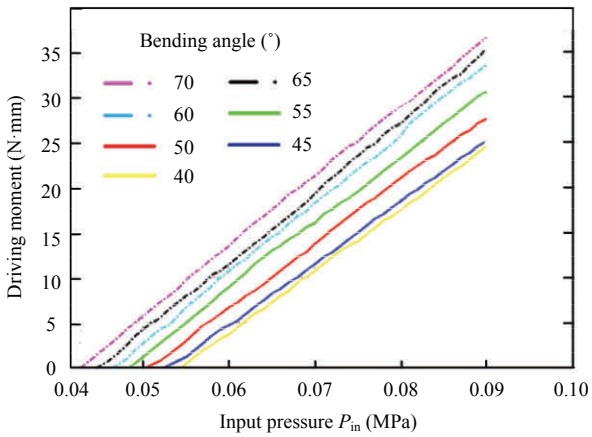

Fig. 5 The P_{in}-M_D characteristic curve of the articulated pneumatic soft actuator.

the propulsion stage is divided into three sub-stages, as shown in Fig. 6. In sub-stage 1, the elbow joint of the forelimb and the hip joint of the hind limb move simultaneously, the elbow joint drives the flipper to achieve full extension, and the hip joint drives the flipper perpendicular to the direction of movement of the robot. In sub-phase 2, the extension joints are coordinated so that the flipper is always perpendicular to the direction of movement to generate propulsive force until the hip and knee joints are fully extended. In sub-stage 3, the ankle joint of the hind limb continues to stretch until the flipper is parallel to the direction of movement of the robot.

The limbs mainly perform intense stretching exercises during the propulsion stage. The ankle joint generally first undergoes a process of acceleration and then deceleration, the acceleration time is very short, and the acceleration trajectory is close to a sine function[11]. The following segmented sine function is used in each sub-stage to represent the acceleration characteristics of the joints:

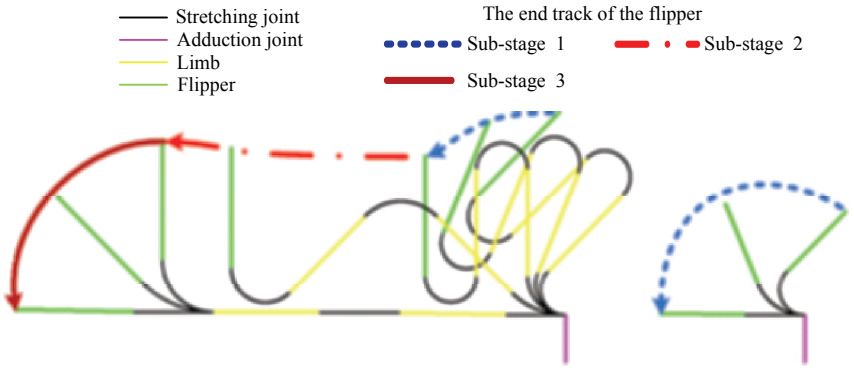

Fig. 6 Joint trajectory planning during the propulsion stage.

$$\begin{cases} \ddot{\theta} = \dfrac{\pi A_{\mathrm{ri}}}{(T_{\mathrm{ai}} + T_{\mathrm{di}})T_{\mathrm{ai}}} \sin\left(\dfrac{\pi}{T_{\mathrm{ai}}} t\right) (0 \le t < T_{\mathrm{ai}}) \\ \ddot{\theta} = \dfrac{\pi A_{\mathrm{ri}}}{(T_{\mathrm{ai}} + T_{\mathrm{di}})T_{\mathrm{di}}} \sin\left[\dfrac{\pi}{T_{\mathrm{di}}}(t - T_{\mathrm{ai}})\right] (T_{\mathrm{ai}} \le t < T_{\mathrm{ai}} + T_{\mathrm{di}}) \end{cases}, \quad (1)$$
$$T_{\mathrm{si}} = T_{\mathrm{ai}} + T_{\mathrm{di}} \, (i = 1, 2, 3),$$

where $\ddot{\theta}$ is the acceleration of the joint; A_{ri} is the movement angle of the joint of a single sub-phase; T_{ai} and T_{di} are the time taken for joint acceleration and deceleration, respectively; and T_{si} is the period of joint motion.

The integral of the segmented sinusoidal acceleration curve on T_{si} is zero to ensure that the limbs have zero velocity at the beginning and end of each sub-phase. In sub-stage 2, the joint deflection angles of the hind limbs have the following equality relationship:

$$\begin{cases} \theta_{\mathrm{ankle}} + \theta_{\mathrm{hip}} - \theta_{\mathrm{knee}} = 90^{\circ} \\ \theta_{\mathrm{hip}} - 90^{\circ} = \theta_{\mathrm{ankle}} \end{cases}, \quad (2)$$

where θ_{ankle} is the deflection angle of the ankle joint; θ_{hip} is the deflection angle of the hip joint; θ_{knee} is the deflection angle of the knee joint.

Thus, the relationship between the joint accelerations of the hind limbs in sub-stage 2 is:

$$\begin{cases} \ddot{\theta}_{\mathrm{ankle}} + \ddot{\theta}_{\mathrm{hip}} - \ddot{\theta}_{\mathrm{knee}} = 0 \\ \ddot{\theta}_{\mathrm{hip}} = \ddot{\theta}_{\mathrm{ankle}} \end{cases}, \quad (3)$$

where $\ddot{\theta}_{\mathrm{ankle}}$ is the acceleration of the ankle joint; $\ddot{\theta}_{\mathrm{hip}}$ is the acceleration of the hip joint; $\ddot{\theta}_{\mathrm{knee}}$ is the acceleration of the knee joint.

According to the planning of the overall form of movement of the joints during the propulsion stage, the total time of the propulsion stage is specified as 1 s, and that of sub-phases 1 and 3 is 0.2 s. The acceleration motion period T_{ai} in the sinusoidal segmentation function of joint acceleration accounts for 30% of the total period T_{si} of the joint motion. The determined acceleration, velocity and angular motion trajectories of the joints are shown in Fig. 7.

3.2 Joint trajectory planning during the recovery stage

The trajectory planning of the recovery stage is also divided into three sub-stages, as shown in Fig. 8. In sub-stage 1, the extension joints are coordinated to achieve the recovery movement, and the flipper is always kept parallel to the direction of the robot movement until the knee joint is completely restored to the original state to minimize the resistance during the limb recovery movement. In sub-stage 2, the ankle joint is fully restored to its original state. In sub-stage 3, the elbow joint and the hip joint move simultaneously until the original state is fully restored.

According to the above description, in sub-phase 1 of the recovery stage, the deflection angles of the joints of the hind limbs have the following equality relationship:

$$\begin{cases} \theta_{\mathrm{ankle}} + \theta_{\mathrm{hip}} - \theta_{\mathrm{knee}} = 180^{\circ} \\ \theta_{\mathrm{hip}} = \theta_{\mathrm{ankle}} \end{cases}. \quad (4)$$

Thus, the relationship between the joint speeds of the hind limbs in sub-stage 1 is:

$$\begin{cases} \dot{\theta}_{\mathrm{ankle}} + \dot{\theta}_{\mathrm{hip}} - \dot{\theta}_{\mathrm{knee}} = 0 \\ \dot{\theta}_{\mathrm{hip}} = \dot{\theta}_{\mathrm{ankle}} \end{cases}, \quad (5)$$

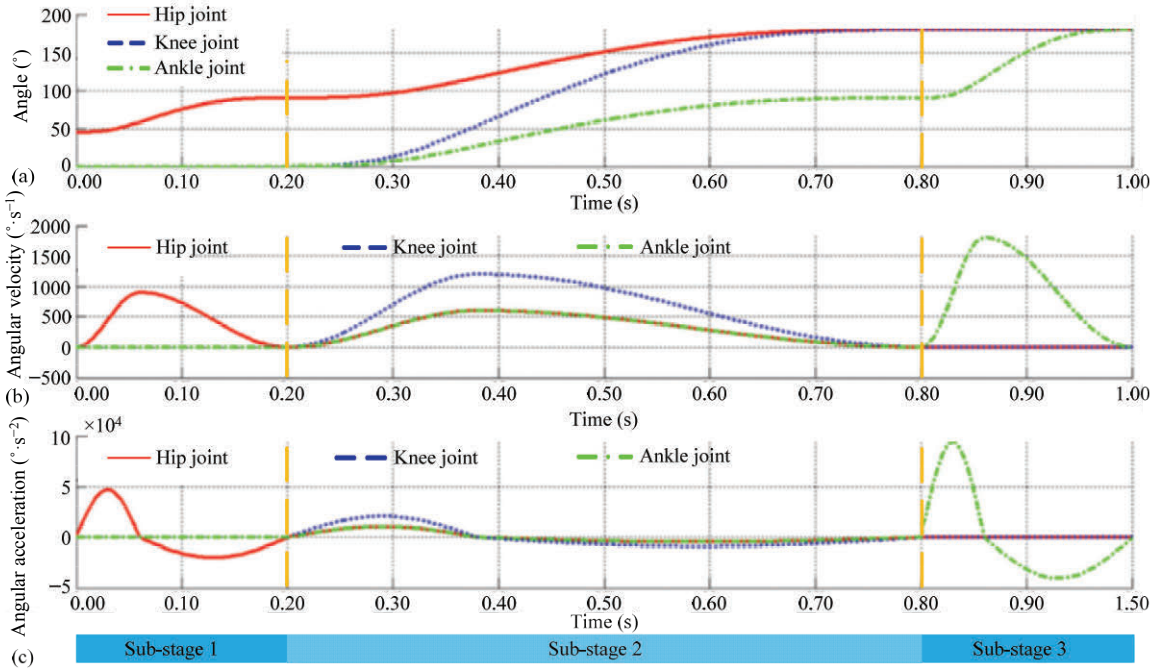

Fig. 7 The trajectory planning result of the propulsion stage. (a) The joint angle of the propulsion phase; (b) the joint angular velocity of the propulsion phase; (c) the joint angular acceleration of the propulsion phase.

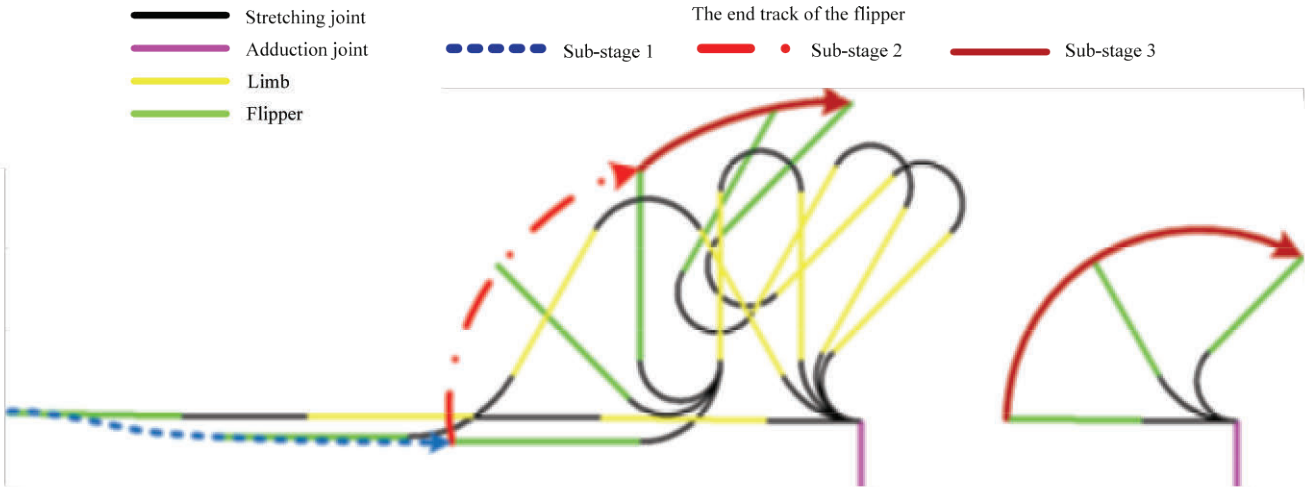

Fig. 8 Joint trajectory planning during the recovery stage.

where $\dot{\theta}_{\text{ankle}}$ is the speed of ankle joint; $\dot{\theta}_{\text{hip}}$ is the speed of hip joint; $\dot{\theta}_{\text{knee}}$ is the speed of knee joint.

According to observation of the frog swimming movement, the time of the recovery stage is set to be three times that of the propulsion stage. Taking the hip joint as an example, a five-degree polynomial fit is applied to the hip joint's motion angle in each sub-stage as Eq. (6).

$$\theta_k(t) = \begin{cases} a_{k1}t^5 + b_{k1}t^4 + c_{k1}t^3 + d_{k1}t^2 + e_{k1}t + f_{k1} \left(0 \le t \le T_{\text{h1}}\right) \\ 90^\circ \left(T_{h1} \le t \le T_{h2}\right) \\ a_{k3}t^5 + b_{k3}t^4 + c_{k3}t^3 + d_{k3}t^2 + e_{k3}t + f_{k3} \left(T_{h2} \le t \le T_{h3}\right) \end{cases},$$
$$t_3 = t - \left(T_{h1} + T_{h2}\right), \tag{6}$$

where t is the swimming time, θ_k is the movement angle of the hip joint and T_{hi} (i = 1, 2, 3) are the time nodes of the different sub-phases, where T_{h1} = 1.5 s, T_{h2} = 0.75 s, and T_{h3} = 0.75 s.

During the recovery stage, the movement of the limbs is relatively flat, the moments of switching between the different sub-stages all adopt a gentle excess acceleration, and the joint speed is zero in the switching of the different stages. To prevent the leg from acting opposite to the direction of the propulsion movement during the recovery phase, the following boundary conditions for the joint trajectory corresponding to Eq. (6) are set:

$$\begin{cases} \theta_{k1}\left(T_{i-1}\right)=\theta_{k(i-1)s} \\ \theta_{k1}\left(T_i\right)=\theta_{kie} \\ \theta_{k1}\left(\dot{T}_{i-1}\right)=0 \\ \theta_{k1}\left(\dot{T}_i\right)=0 \\ \theta_{k1}\left(\ddot{T}_{i-1}\right)=0 \\ \theta_{k1}\left(\ddot{T}_i\right)=0 \end{cases} \quad (i=1,2,3), \qquad T_0=0, \tag{7}$$

where $\theta_{k(i-1)s}$ and θ_{kie} are the angles of the joints at the beginning and end of the different sub-phases, respectively.

The curves of the joint angle, angular velocity and acceleration characteristics of the recovery stage can be obtained by the above analysis, as shown in Fig. 9. The joint movement curves of the limbs are smooth during the entire recovery stage, and those of the sub-stages are smooth and excessive, with no sudden changes in acceleration and speed.

3.3 Actuator control strategy

To realize frog-like movement, an incremental PID controller based on air pressure feedback is established to control the motion behavior of each joint. The control process of a single actuator is shown in Fig. 10a.

The reference angle θ of the controlled joint is obtained by trajectory planning. Combined with the motion characteristics, the expected air pressure in the inner cavity of the actuator for achieving the reference angle is obtained. The deviation between the expected and actual air pressure values is sent to the PID controller, and the control amount u is output. The control amount controls the opening degree of the solenoid valve by controlling the duty ratio and adjusts the air pressure to realize closed-loop control of the actuator. According to the response speed of the actuator, the control period of a single PID is determined to be 20 ms, and the air pressure trajectory curve is shown in Fig. 10b. There is no hysteresis in the curve, which satisfies the control requirements.

4 Prototype experiments

4.1 Structural verification experiment

The structure and control system are integrated to build a prototype of the frog-inspired swimming robot. The overall mass is 1.29 kg, the torso size is 0.175 m × 0.1 m × 0.06 m, the length of the hind limbs is 0.152 m when fully extended and the areas of the front and hind flippers are 0.003 m^2 and 0.05 m^2, respectively.

The robot is placed on land, and the overall performance of the robot is debugged through the control system. The action series is shown in Fig. 11. The robot is flexible in the movement process, and the action execution is basically consistent with the previous planning procedure. The propulsion motion is realized based on the articulated pneumatic soft actuator, which preliminarily verifies the rationality of the trajectory planning.

4.2 Linear motion experiment

Post-processing of the captured experimental video is used to obtain the swimming posture sequence of the robot, wherein the starting position of the robot is marked as “Start”, the position is fixed in the figure, and the end position is marked as “End”. The shaded portion of the last picture represents the absolute position of the robot in the initial stage.

The linear swimming sequence of linear motion is shown in Fig. 12. The duration of a single swim is approximately 6 s. The propulsion distance is approximately 0.45 m, which is twice the length of its own body; and the average propulsion speed is approximately 0.075 $m \cdot s^{-1}$. Motion analysis reveals that the joints move at the same time during the advancing movement, and the flippers are driven to perform stroke movements from the outside to the inside. The form of movement is similar to that of an aquatic frog based on lift, and the

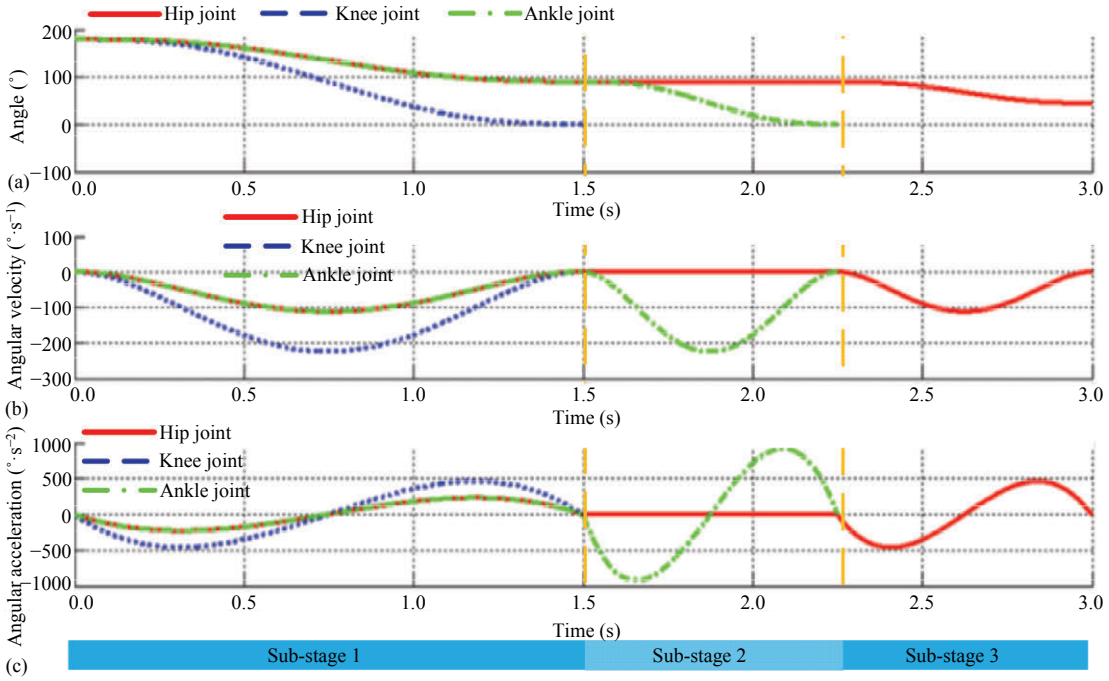

Fig. 9 The trajectory planning result of the recovery stage. (a) The joint angle of the recovery phase; (b) The joint angular velocity of the recovery; (c) The joint angular acceleration of the recovery.

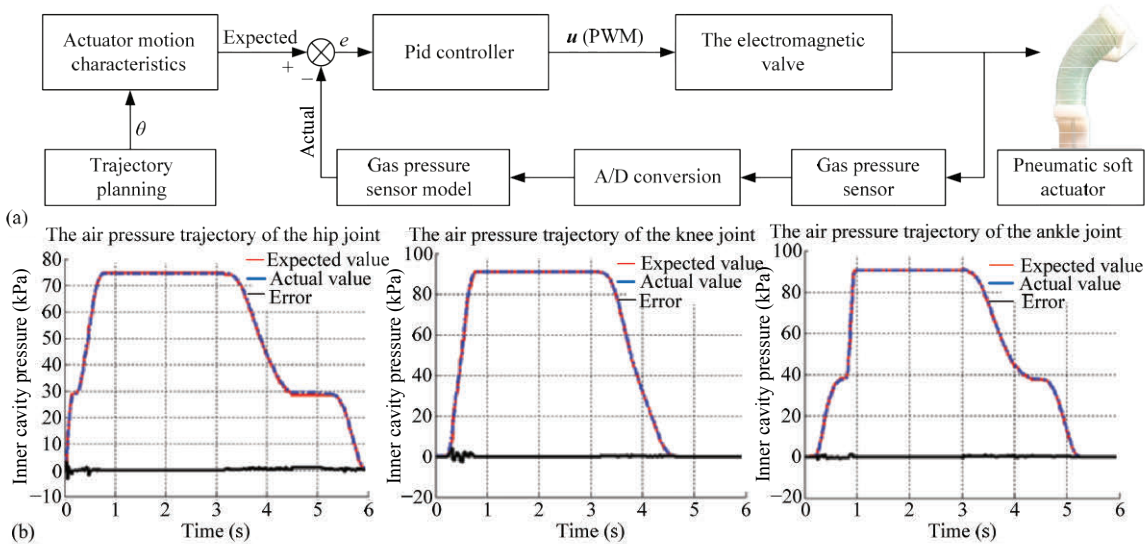

Fig. 10 The control principle and air pressure characteristic curve of soft actuator.

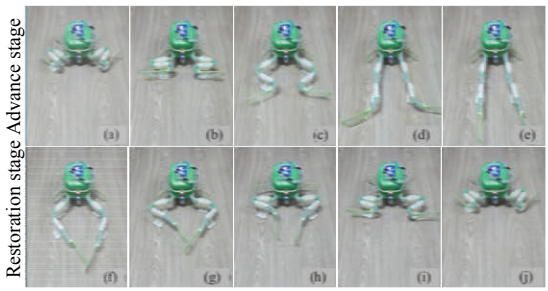

Fig. 11 The simulated swimming experiment of the prototype on land.

last moment of the propulsion phase is more severe. In addition, the robot has better motion stability during the linear motion process, which preliminarily verifies the rationality of the structure.

4.3 Turning motion experiment

The yaw moment generated by the coordinated motion of the four limbs can realize the turning motion. A left-turn motion sequence and the internal air pressure characteristic curve of each joint actuator are shown in

Fig. 13. In the initial stage, the coordinated movement of the limbs achieves a short-term linear motion to break the water resistance, and then use the driving force generated by the propulsion of a single hind limb. In the recovery process, the knee joint is first retracted, and the hind limbs continue to stroke with the driving of the knee joint; this process continuously provides driving torque for the turning motion, and the other joints finally

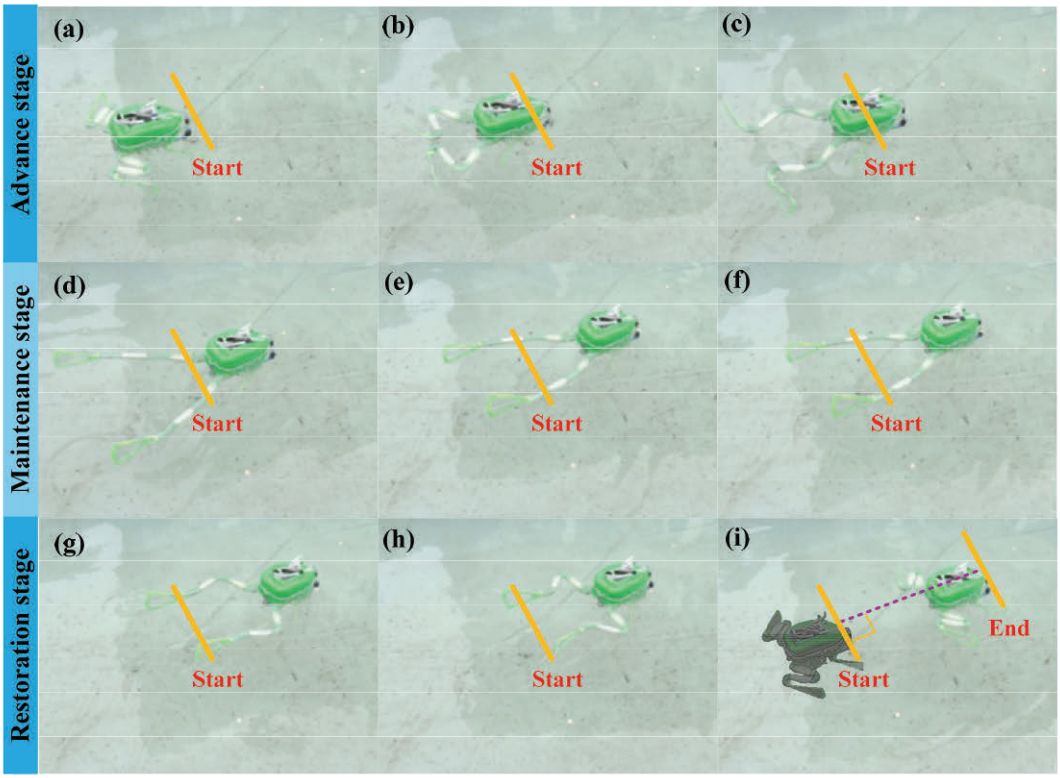

Fig. 12 The sequence of motions in which the limbs advance linear motion.

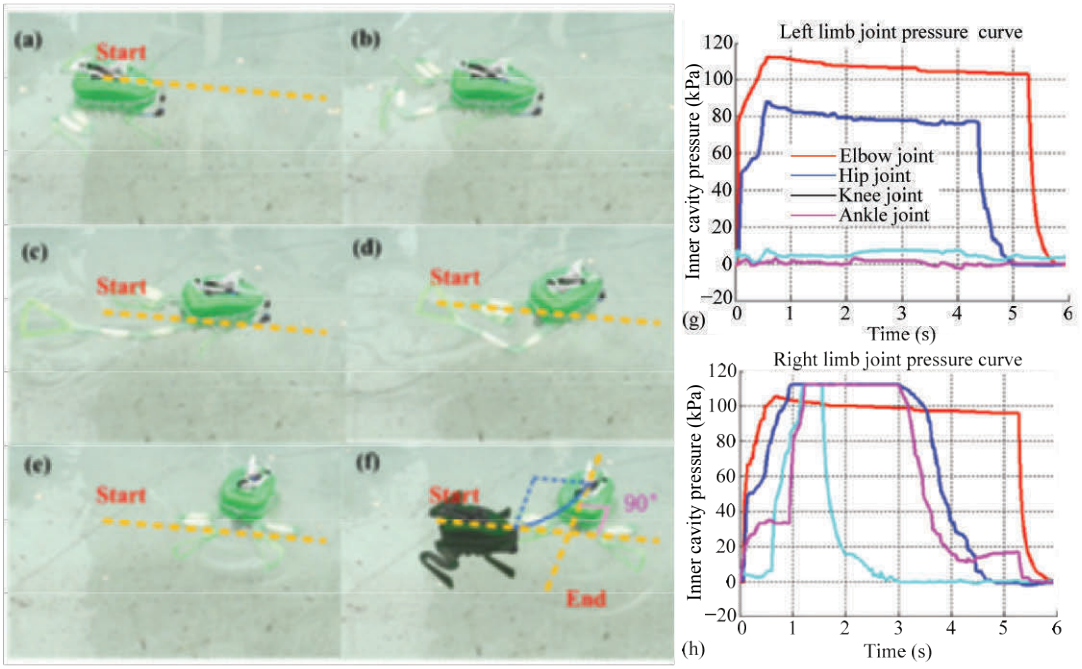

Fig. 13 The sequence of actions when turning to the left the air pressure characteristic curve of each joint actuator when turning to the left.

return to the initial state. The angle of a single turn can reach 90°, the average turning speed is 15 $^{\circ}\cdot s^{-1}$ and the turning radius is 0.20 m. The principle of turning right is similar to that of turning left.

5 Conclusions and future work

A frog-inspired swimming robot based on articulated pneumatic soft actuators is presented to enhance its environmental adaptability. The fusion of rigid and soft materials not only ensures sufficient toughness but also realizes the miniaturization of the robot. The mould structure of a soft actuator and its manufacturing process are designed. Based on characteristic analysis of the actuator, the joint trajectory is planned in the form of joint angle, angular velocity and angular acceleration. Frog-like movement is realized by the coordination of the actuators, which shows that the structure and trajectory planning are reasonable. The robot can propel forward a distance of 0.45 m, which is twice the length of its own body. A single turning angle can reach 90°, and the turning radius is approximately 0.20 m. In future work, we intend to develop a frog-inspired robot with amphibious capabilities by improving the structural model and drive unit.

Acknowledgment

This work is supported by the National Key Research and Development Plan (2017YFB1300104) and National Natural Science Foundation of China (Grant No. 51675124).

* All supplementary materials are available at https://doi.org/10.1007/s42235-020-0021-8.

References

[1] Wehner M, Truby R L, Fitzgerald D J, Mosadegh B, Whitesides G M, Lewis J A, Wood R J. An integrated design and fabrication strategy for entirely soft, autonomous robots. *Nature*, 2016, **536**, 451–455.

[2] Li T, Yang M Z. Mechanism design and kinematics analysis of frog-like jumping robot. *Machinery*, 2009, **36**, S119–S120. (in Chinese)

[3] Wang M, Zang X Z, Fan J Z, Zhao J. Biological jumping mechanism analysis and modeling for frog robot. *Journal of Bionics Engineering*, 2008, **5**, 181–188.

[4] Eshgi S, Azimirad V, Hajimohammadi H. Design and modeling of a new biomimetic robot frog with the ability of jumping altitude regulation. In: *Biomimetic and Biohybrid Systems*, Prescott T J, Lepora N F, Mura A, Verschure P F M J, eds., *Springer*, Berlin, Heidelberg, Germany, 2012.

[5] Richards C T. Kinematics and hydrodynamics analysis of swimming anurans reveals striking inter-specific differences in the mechanism for producing thrust. *Journal of Experimental Biology*, 2010, **213**, 621–634.

[6] Nguyen P L, Do V P, Lee B R. Dynamic modeling and experiment of a fish robot with a flexible tail fin. *Journal of Bionic Engineering*, 2013, **10**, 39–45.

[7] Richards C T. The kinematic determinants of anuran swimming performance: An inverse and forward dynamics approach. *Journal of Experimental Biology*, 2008, **211**, 3181–3194.

[8] Pandey J, Reddy N S, Ray R, Shome S N. Multi-body dynamics of a swimming frog – A Co-simulation approach. *IEEE International Conference on Robotics and Biomimetics*, Shenzhen, China, 2013, 842–847.

[9] Pandey J, Reddy N S, Ray R, Shome S N. Biological swimming mechanism analysis and design of robotic frog. *IEEE International Conference on Mechatronics and Automation*, Takamatsu, Japan, 2013, 1726–1731.

[10] Fan J Z, Zhang W, Kong P C, Cai H G, Liu G F. Design and dynamic model of a frog-inspired swimming robot powered by pneumatic muscles. *Chinese Journal of Mechanical Engineering*, 2017, **30**, 1123–1132.

[11] Zhang W. *Research on the Frog Inspired Robot and Its Swimming Trajectory Planning*, PhD thesis, Harbin Institute of Technology, Harbin, China, 2017. (in Chinese)

[12] Tang Y C, Qin L, Li X N, Chew C M, Zhu J. A frog-inspired swimming robot based on dielectric elastomer actuators. *IEEE/RSJ International Conference on Intelligent Robots and Systems*, Vancouver, Canada, 2017, 2403–2408.

[13] Rus D, Tolley M T. Design, fabrication and control of soft robots. *Nature*, 2015, **521**, 467–475.

[14] Laschi C, Mazzolai B, Cianchetti M. Soft robotics: Technologies and systems pushing the boundaries of robot abilities. *Science Robotics*, 2016, **1**, eaah3690.

[15] Sholl N, Moss A, Kier W M, Mohseni K. A soft end effector inspired by cephalopod suckers and augmented by a dielectric elastomer actuator. *Soft Robotics*, 2019, **6**, 356–367.

[16] Chen B X, Jiang H Z. Swimming performance of a tensegrity robotic fish. *Soft Robotics*, 2019, **6**, 520–531.

[17] Li T F, Zou Z N, Mao G Y, Yang X X, Liang Y M, Li C, Qu S X, Suo Z G, Yang W. Agile and resilient insect-scale robot.

Soft Robotics, 2018, **6**, 133–141.

[18] Zhou X B, Teng Y, Li X N. Development of a new pneumatic-driven earthworm-like soft robot. 23*rd International Conference on Mechatronics and Machine Vision in Practice* (*M2VIP*), Nanjing, China, 2016, 50–54.

[19] Hao Y F, Gong Z Y, Xie Z X, Guan S Y, Yang X B, Ren Z Y, Wang T M, Wen L. Universal soft pneumatic robotic gripper with variable effective length. 35*th Chinese Control Conference*, Chengdu, China, 2016, 6109–6114.

[20] Yan H, Su Y M, Yang L. Experimentation of fish swimming based on tracking locomotion locus. *Journal of Bionic Engineering*, 2008, **5**, 258–263.

[21] Han L B, Wang Z Y, Ji A H, Dai Z D. The mechanics and trajectory control in locust jumping. *Journal of Bionic Engineering*, 2013, **10**, 194–200.

[22] Wei Z, Liu G F, Fan J Z, Cai H G. Foot trajectory planning of frog swimming based on propulsion mechanism. *IEEE International Conference on Robotics & Biomimetics*, Zhuhai, China, 2015.

[23] Bazaz S A, Tondu B. Optimization of a robotic manipulator joint trajectory travel time with velocity and acceleration constraints. *Proceedings of the IEEE International Symposium on Assembly and Task Planning*, Marina del Rey, USA, 1997.

[24] Bazaz S A, Tondu B. Minimum time online joint trajectory generator based on low order spline method of industrial manipulators. *Robotics and Autonomous Systems*, 1999, **29**, 257–268.

[25] Fan Z H. *Research on Jumping Robot Based on Skeletal Structure of the Frog*, MS thesis, Harbin Institute of Technology, Harbin, China, 2016. (in Chinese)

[26] Dong H B. *Research on Key Technologies of a Pneumatic Soft Omnidirectional Bending Module*, MS thesis, Harbin Institute of Technology, Harbin, China, 2016. (in Chinese)

[27] Polygerinos P, Wang Z, Galloway K C, Wood R J, Walsh C J. Soft robotic glove for combined assistance and at-home rehabilitation. *Robotics and Autonomous Systems*, 2015, **73**, 135–143.

[28] Zhang W, Fan J Z, Zhu Y H, Qiu Y L, Zhao J. A method for mechanism analysis of frog swimming based on motion observation experiments. *Advances in Mechanical Engineering*, 2015, **6**, 403057.

[29] Peters S E, Kamel L T, Bashor D P. Hopping and swimming in the leopard frog, Rana pipiens: I. Step cycles and kinematics. *Journal of Morphology*, 1996, **230**, 1–16.

[30] Kong P C. *Research on Design and Key Technologies of Frog-inspired Swimming Robot Actuated by Pneumatic Muscles*, MS thesis, Harbin Institute of Technology, Harbin, China, 2016. (in Chinese)